Hindawi
Journal of Advanced Transportation
Volume 2024, Article ID 3138719, 19 pages
https://doi.org/10.1155/2024/3138719

Research Article

Exploring the Impact of Rainfall on Vehicle Trajectory Patterns and Sideslip Risk: An Empirical Investigation

Bo Wang,[1,2,3] **Yiik Diew Wong**,[2] **Chi Zhang**,[1,3] **Hong Zhang**,[4] **and Yanyang Gao**[1,3]

[1]*School of Highway, Chang'an University, Xi'an 710000, China*
[2]*School of Civil and Environmental Engineering, Nanyang Technological University, Singapore 639798, Singapore*
[3]*Engineering Research Center of Highway Infrastructure Digitalization, Ministry of Education, Xi'an 710000, China*
[4]*Transportation Institute, Inner Mongolia University, Hohhot 010021, China*

Correspondence should be addressed to Yiik Diew Wong; cydwong@ntu.edu.sg and Chi Zhang; zhangchi@chd.edu.cn

Received 31 August 2023; Revised 19 January 2024; Accepted 27 January 2024; Published 3 February 2024

Academic Editor: Maria Castro

Understanding the sideslip risks of various trajectory patterns, as well as the impact of rainfall on them, is critical for improving road safety. However, the lack of precise classification indicators hampers systematic analysis of the variations in vehicle trajectory patterns. To address this, this study proposes a parameterized classification method for trajectories on curved segments, employing the radius and offset of the trajectory as the primary classification features and dividing the trajectories into nine patterns. These patterns represent variations from smaller to larger radii and inside to outside lane offsets, reflecting different driving behaviors and vehicle stability during vehicle cornering. Concurrently, the friction coefficient utilization rate is used to effectively compare vehicles' sideslip risk under different weather conditions. Based on this, we construct a framework using computer vision technology for automatically identifying trajectory patterns and measuring sideslip risk. We conducted an empirical study on a highway-curved segment with high sideslip risk in China and collected two datasets under clear and rainy conditions for analysis. The classification results show that the proposed method can effectively classify trajectories according to nine trajectory patterns. Comparative analysis reveals that vehicle trajectories in both the inside and outside lanes are notably more affected by rainfall compared to the middle lane. Meanwhile, trucks demonstrate a higher susceptibility to rainfall than cars. In addition, the analysis of the sideslip risk for different trajectory patterns discovers several high-risk patterns. This study provides an effective approach for monitoring and analyzing the sideslip risk on curved segments, thereby contributing to the enhancement of road design and traffic safety management.

1. Introduction

Rainfall poses a severe threat to highway driving safety, primarily due to its reduced skid resistance between tires and road pavement and the visibility of vehicles [1, 2]. Among these, the reduced skid resistance is often difficult to detect, causing drivers to overlook the crash risk. Driving on wet roads increases the likelihood of vehicle accidents and intensifies their severity. Fatal traffic crashes are 34% more likely to occur under rainy conditions than in clear weather conditions, and this likelihood increases by 27% even in light rain [3]. About 11% of car crashes and nearly a quarter of fatal cases occur during periods of rainfall each year in Louisiana [4]. The reasons behind the frequent crashes under rainy conditions not only lie in the reduced skid resistance leading to longer braking distances for vehicles but also in the fact that vehicles easily sideslip on curved segments [5]. Previous studies have shown that rainfall can increase the expected number of severe crashes on curved segments by 3.26 times [6, 7]. Therefore, comprehending the impact of rainfall on vehicle sideslip risk on curved segments is crucial for enhancing road design and traffic safety management.

Factors affecting the sideslip risk on curved segments under rainy conditions mainly include road surface conditions [8], road geometry [9, 10], vehicle performance [11], and

rainfall [12]. Previous studies have achieved many results by extensively investigating these factors using various methods, such as crash report data [13, 14], simulation experiments [15, 16], and actual vehicle experiments [17]. However, crash report data cannot reveal the impact of rainfall on vehicle sideslip risk at the microlevel. Meanwhile, there are limitations in the data quantity and quality of simulation experiments and actual vehicle experiments. Researchers are turning to mass-collected trajectory data under naturalistic driving conditions [18, 19]. Based on this, the impact of rainfall on vehicles has been analyzed using more microscopic indicators from trajectories, including speed, lateral acceleration, lateral offset of vehicles, and intervehicle distance [20, 21]. Nevertheless, previous studies have overly focused on the trajectories of a small number of abnormal vehicles, neglecting the overall changes in trajectory features [22, 23]. The classification of trajectory patterns is an essential basis for observing the overall changes in trajectory features. Previous studies have explored methods for classifying trajectories on curved segments, encompassing both single-indicator-based and mixed classification methods. The single-indicator-based classifications, such as trajectory radius [24], lane departure [25], and curve-cutting position [26], offer specific advantages such as effective sideslip risk description, simplicity and practicality, and utilization of turning characteristics, respectively. On the other hand, mixed classification [27], exemplifying patterns such as cutting, swinging, drifting, correcting, and normal and ideal behavior, provides a systematic categorization of vehicle trajectories on curved segments, being widely utilized despite its limitations in precise indicator definition and potential overlap in trajectory categories. However, the classification methods proposed in previous studies still have limitations: (a) some methods are only applicable to specific curved segments (e.g., hairpin curved roads) and cannot be universally applied to all cases; (b) many classifications do not fully consider the characteristics of curved trajectories, namely, the radius of the trajectory and lateral offset; and (c) many classification methods only provide illustrations without giving classification indicators.

With the advancement of computer vision technology, vehicle trajectories can be extracted more accurately from video [28, 29]. This overcomes the limitations of technologies like radar, such as difficulty in coordinate conversion and low data accuracy of trajectories [30]. Consequently, a more detailed and accurate driving behavior analysis based on vehicle trajectories is possible [31, 32]. Although the video collected by drones is more straightforward regarding coordinate conversion, it is difficult to collect video of vehicle movements under rainy conditions. The closed-circuit television (CCTV) systems widely deployed along highways effectively mitigate data collection constraints under rainy conditions. Therefore, this study uses computer vision methods to process road surveillance videos to obtain vehicle trajectories under clear and rainy weather conditions as the databases for this study.

In essence, this study aims to explore the impact of rainfall on the safety of driving on curved segments using real driving trajectory data. To address the gaps in previous research, this study first proposes a parameterized trajectory classification method. It categorizes vehicle trajectories on curved segments into nine patterns based on the trajectory's radius and offset. The proposed method is more explicit and suitable for automated data extraction and processing than previous methods. Meanwhile, the friction coefficient utilization rate is used to effectively compare vehicles' sideslip risk under different weather conditions. Based on this, we construct a framework for automatic trajectory pattern identification and sideslip risk measurement based on machine vision technology. We use it to collect two datasets of the same curve under clear and rainy conditions, containing the trajectories of 970 and 1021 vehicles, respectively. Based on these datasets, we investigated the proportion and safety of trajectory patterns under clear versus rainy weather conditions. This study has the following two-fold contributions: First, at the methodological level, we proposed a parametric classification method for the trajectories on curved segments. This method fills the void of quantitative indices in previous trajectory classifications and enables a more accurate analysis of trajectory characteristics. Simultaneously, it facilitates the swift identification of vehicle trajectory patterns using computer vision technology. Secondly, at the application level, we extensively analyze the various vehicle trajectory patterns, revealing the strategies employed by drivers to safely navigate curved segments during rainfall. This innovative approach would facilitate enhancing the design of highway curved segments and optimizing traffic management strategies.

The rest of the paper is structured as follows. Section 2 provides a literature review. Section 3 introduces the methodology. Section 4 gives the data preparation and implementation details. The results and discussion are presented in Section 5. Finally, Section 6 provides the conclusions of our work.

2. Literature Review

2.1. Sideslip Risk Measurement. Vehicle sideslip, a dangerous situation of lateral vehicle instability, is most common when a vehicle passes around a curved segment [33]. The vehicle may sideslip if the friction between the tires and the road surface is insufficient to counteract the centrifugal force during vehicular curve driving. Figure 1 shows a typical example of a vehicle sideslip on a highway curve. Sideslip risk measurement indicators generally fall into two categories based on vehicle states [34, 35] and based on friction coefficient [36, 37]. Among the indicators based on vehicle status, the sideslip angle provides the most direct reflection of the sideslip condition, which is defined as the angle between the actual direction of vehicle motion and the wheel orientation. However, a significant drawback of the sideslip angle is its delayed response, as its value increases abruptly only when the sideslip occurs [37]. To measure the sideslip risk of a vehicle before the sideslip occurs, Chen et al. [15] proposed the sideslip index, which can indicate the risk trend before the sideslip occurs based on tire loads. However, such indicators are usually only available for simulation models or sensor-equipped vehicles due to the difficulty of obtaining vehicle state data.

Figure 1: Example of a vehicle sideslip. The white car sideslipped and lost control, eventually crashing into the orange car. During this incident, the white car corrected its direction twice. (a) Normal state. (b) Sideslip. (c) First correction. (d) Lost control. (e) Second correction.

Compared to vehicle state-based measurement, friction coefficient-based measurement is better suited for practical road design and maintenance work [15]. The friction coefficient of the road surface is directly utilized to measure its skid resistance performance [38]. Furthermore, the friction coefficient required for maintaining vehicle balance can be estimated based on the vehicle's speed and motion radius. Road geometry design extensively applies the required friction coefficient [39]. However, it is less used in measuring real vehicle sideslip risk. This is because it necessitates real-time data on the vehicle's trajectory, radius, and speed. Nevertheless, the required friction coefficient of the vehicle provides a metric foundation for employing computer vision to measure vehicle sideslip risk [40, 41].

2.2. Trajectories Classification. Regarding geometric characteristics, curved segment trajectories display more distinct feature variations than straight segments. Currently, there are mainly two types of classification methods for curved segment vehicle trajectory patterns: one is based on single indicators, such as the trajectory radius [42] and lane departure [43]; the other is mixed classification method [44], which is the most commonly applied method, and categorizes the trajectories into six patterns, as shown in Figure 2. In addition, Table 1 presents a detailed analysis of four representative classification methods for curved segment trajectories, examining their advantages and disadvantages.

According to the analysis results in Table 1 and the literature review, we identify three aspects where current trajectory classification methods need improvement to observe the overall variation of trajectory characteristics more effectively. (a) Enhancing the universality of classification methods. For example, the method "based on the position of the curve-cutting point" is mainly applicable to specific road scenarios like "hairpin curves." (b) Integrating the characteristics of curved trajectories. For instance, the "based on lane departure" and the mixed classification methods show poor correlation with the characteristics of curved trajectories. (c) Defining precise classification indicators. For example, the mixed classification method lacks clear classification indicators, and many trajectory categories overlap, making it difficult to distinguish effectively.

3. Methodology

In this study, a framework for vehicle trajectory pattern identification and sideslip risk measurement in curved segments is developed based on computer vision technology, as shown in Figure 3. The framework consists of three parts: (1) trajectory extraction; (2) trajectory pattern classification; and (3) sideslip risk measurement. Subsequent subsections present each of these components in Sections 3.1–3.3 in their respective order.

3.1. Trajectory Extraction. In the trajectory extraction part, we employ computer vision techniques to extract vehicle trajectories from surveillance videos. Specifically, this process can be divided into three steps. Firstly, we conduct vehicle detection and tracking to automatically capture the vehicle trajectories from videos in the image coordinate system. Secondly, we conduct camera calibration and coordinate transformation to convert trajectory coordinates into real-world coordinates based on the camera parameters.

3.1.1. Vehicle Detection and Tracking. In step 1, we employ the YOLO (You Only Look Once) and StrongSORT algorithms to achieve automated vehicle detection and tracking. YOLO, as a leading vehicle detection algorithm currently [47, 48], utilizes a single neural network to predict the bounding box and class probabilities of each object in a single forward pass. Compared to region-based convolutional neural network (R-CNN), YOLO algorithm boasts advantages of faster detection speed and easier deployment [49]. Moreover, to maintain continuous vehicle trajectory tracking, it is necessary to integrate vehicle detection algorithms with multiobject tracking (MOT) algorithms. StrongSORT, as an advanced MOT algorithm, integrates Gaussian-smoothed interpolation (GSI) with DeepSORT to reduce detection loss effectively [50]. In this study, we trained Yolo v5 Version 6.0 and StrongSORT V4.0 models based on a dataset of more than 12,000 vehicles. The snapshot of object detection and tracking uses YOLO and Deep Sort, as shown in Figures 3(a) and 3(b).

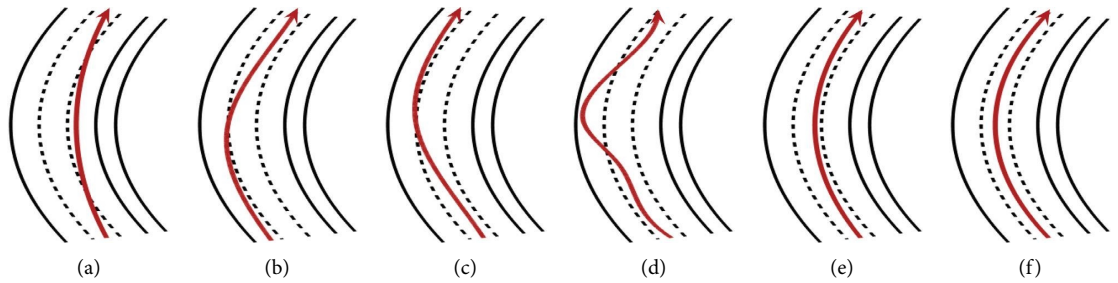

Figure 2: Schematic diagram of trajectory patterns based on the mixed classification method. (a) Cutting. (b) Swinging. (c) Drifting. (d) Correcting. (e) Normal behavior. (f) Ideal behavior.

3.1.2. Camera Calibration and Coordinate Transformation. In step 2, the trajectory data obtained in the image coordinate system (u-v coordinates) must be further converted into Frenet coordinates (s-d coordinate system) for better visualization and classification of the trajectories. By utilizing the spatial position and focal length of the surveillance camera, the mapping relationship between the image coordinate system and the world coordinate system can be deduced, as shown in (1) [51]. Thus, accurate external parameters of the surveillance camera, such as focal length, rotation angle, pitch angle, and height, are crucial for coordinate transformation. Various camera parameter calibration methods have been applied in previous studies, which can be divided into multivanishing point methods and single-vanishing point methods [52]. Due to the lack of effective reference objects on road segments, this study combines the previous research results to apply the "VWL" (one vanishing point, known width and length) method for camera parameter calibration [53, 54]. The "VWL" method determines a vanishing point based on the road markings and then obtains the camera parameters based on the known length of the road markings and a set of parallel markings with known spacing, as shown in equations (2)–(6) and Figure 4(a).

$$\begin{bmatrix} \xi u \\ \xi v \\ \xi \end{bmatrix} = \begin{bmatrix} f\cos\sigma & -f\sin\sigma & 0 & 0 \\ -f\sin\phi\sin\sigma & -f\sin\phi\cos\sigma & -f\cos\phi & fh\cos\phi \\ \cos\phi\sin\sigma & \cos\phi\cos\sigma & -\sin\phi & h\sin\phi \end{bmatrix} \begin{bmatrix} x \\ y \\ z \\ 1 \end{bmatrix}, \tag{1}$$

$$h = \frac{fw\sin\phi}{\Delta u\cos\sigma}, \tag{2}$$

$$f = \frac{v_0}{\tan\phi}, \tag{3}$$

$$\phi = \arcsin\left(\frac{v_0\tan\sigma}{u_0}\right), \tag{4}$$

$$\sigma = \frac{\arcsin T}{2}, \tag{5}$$

$$T = \frac{2v_0 w}{L\Delta u}\left(\frac{u_i}{v_0 - v_i} - \frac{u_j}{v_0 - v_j}\right)\left(v_i > v_j\right), \tag{6}$$

where (u, v) represents the coordinate values in the image coordinate system, and (x, y, z) represents the coordinate values in the world coordinate system. f is the camera focal length, σ is the camera rotation angle, ϕ is the camera pitch angle, h is the camera height (m), and ξ is the scaling factor. (u_0, v_0) is the vanishing point image coordinate, (u_i, v_i) and (u_j, v_j) are the start and end point image coordinates of the length reference object, Δu is the difference in intercepts of the two known parallel lines on the road in the coordinate axis, W is the distance between the two known parallel lines on the road, L is the actual length (m) of the length reference object, and T is an intermediate variable.

Although some reliable methods have been proposed in previous studies to transform the world coordinate system into

Table 1: Summary of classification methods of trajectory patterns.

Method	Trajectory pattern	Advantage	Disadvantage
Based on the trajectory radius [24, 42]	3 patterns: (a) constant; (b) understeering; and (c) oversteering	This method can effectively describe the sideslip risk of vehicles. When a vehicle is oversteering, the sideslip risk is higher	This method only considers the extreme conditions during turning. In addition, it requires many indicators from the vehicle's steering system. Thus, the observed trajectories cannot be directly classified
Based on lane departure [25, 43]	3 patterns: (a) no lane departure; (b) lane departure to the inside; and (c) lane departure to the outside	This method is both simple and practical, enabling accurate categorization	Merely considering lane deviation is insufficient to fully describe the characteristics of trajectories on curved segments
Based on position of the curve-cutting point [26]	3 patterns: (a) near the middle of the curved segment; (b) near the exit of the curved segment; and (c) near the entry of the curved segment	This method effectively utilizes the turning characteristics of vehicles on curved segments to categorize trajectories	This method lacks precise categorization indicators
Mixed classification [27, 44–46]	6 patterns: (a) cutting; (b) swinging; (c) drifting (d) correcting; (e) normal behavior; and (f) ideal behavior	This method systematically categorizes vehicle trajectories on curved segments. It is also the most widely used classification method	The method lacks precise indicators. At the same time, some trajectory categories overlap and are difficult to distinguish. The characteristics of the trajectory cannot be effectively described

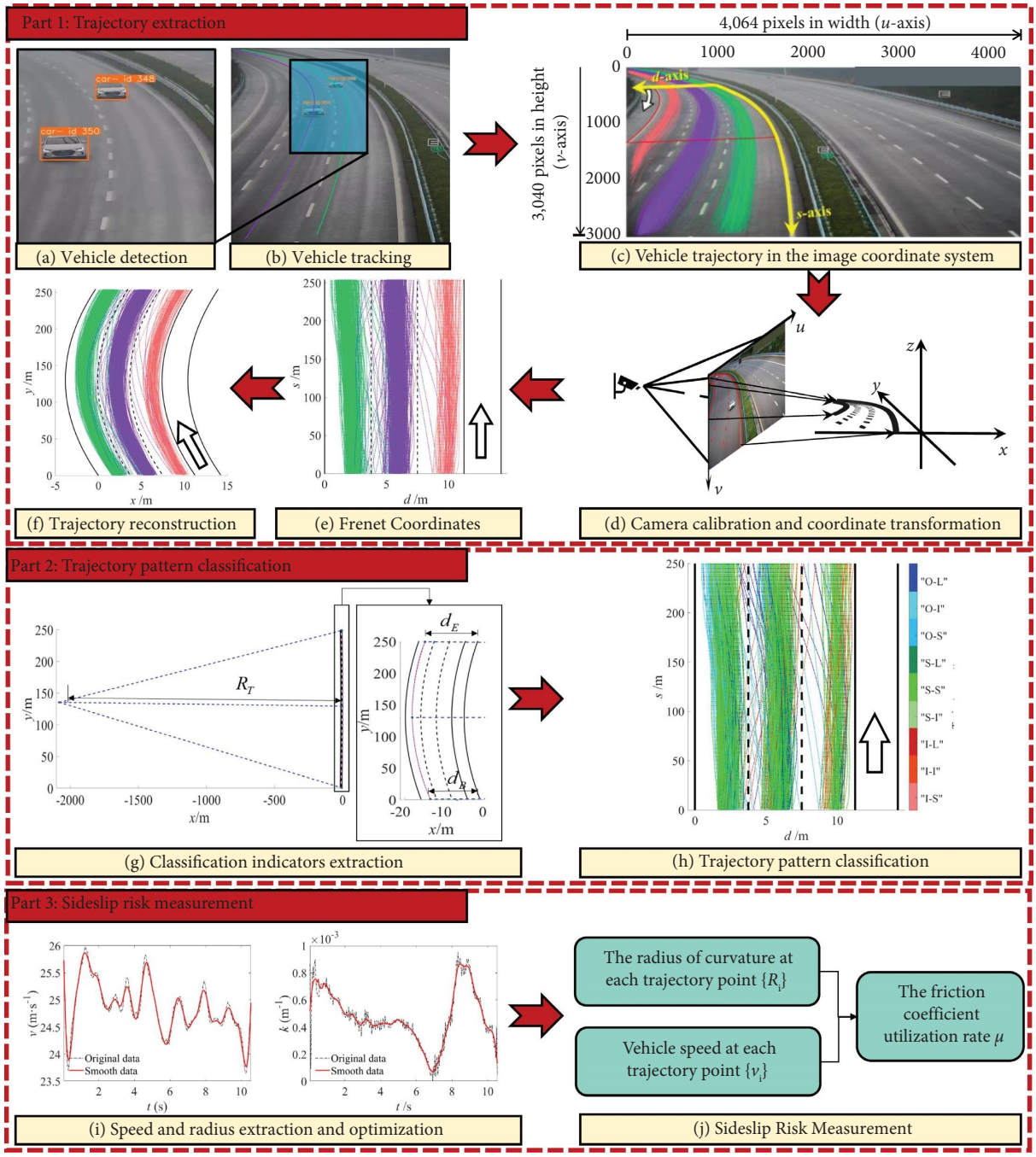

Figure 3: Framework of trajectory pattern identification and sideslip risk measurement based on computer vision.

the Frenet coordinate system [55], significant lens distortion and irregular scaling exist due to the camera perspective of surveillance video. To accurately measure the trajectory in real-world units (e.g., meters), this study adopts a grid remapping method that directly transforms trajectory data from the u-v coordinate system to the s-d coordinate system [56]. Based on the camera calibration results, the grid mesh is established by equation (1). Every grid is of equal size in real-world units, which represents an equal-sized planar area of the actual road. In this study, the grid dimensions are chosen based on the monitored scene's key reference points: the lane width (3.75 m) and road marking length (6.0 m), with the lateral grid width set to 0.1875 m to divide the lane width into 20 units and the longitudinal grid length to 1 m to divide the marking length into six units, as shown in Figure 4(b). Based on this, the trajectory data transformed into an s-d coordinate system, as

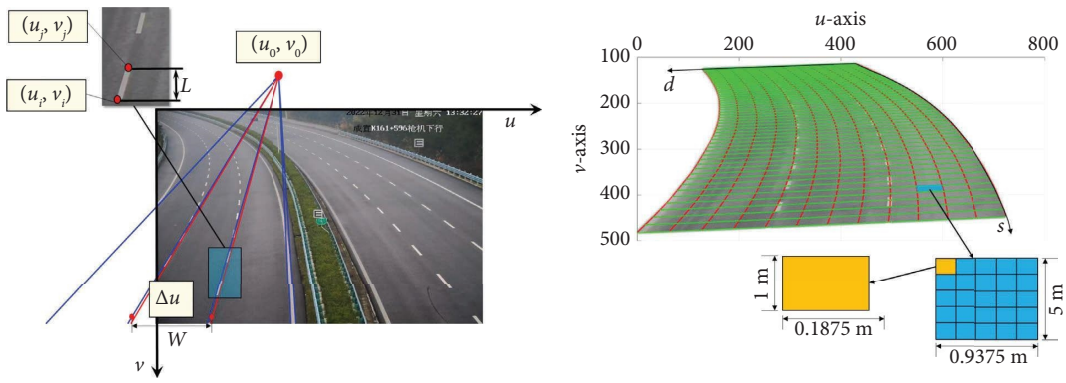

Figure 4: Schematic diagram of camera calibration and grid mesh establishment. (a) "VWL" method for camera parameter calibration. (b) Grid mesh establishment based on camera calibration.

shown in Figure 3(e). Further, according to the road geometry, we reconstruct the vehicle trajectory in the x-y coordinate system, as shown in Figure 3(f).

3.2. Trajectory Pattern Classification

3.2.1. Classification Indicators. To effectively analyze highway driving safety, it is essential to consider the characteristics of the trajectory on curved segments when conducting systematic trajectory classification. The trajectory on curved segments has the following three major characteristics: (a) smooth and continuous; (b) approximated as circular arcs; and (c) possibly offset to one side. The trajectory of a vehicle within a curved segment can be approximated as a circular arc. This circular radius of approximation R_T, referred to as the "trajectory's approximation radius," is a significant characteristic for distinguishing different types of trajectories. For example, the "cutting" and "ideal behavior" trajectory types proposed in previous studies can be differentiated using R_T [57]. In addition, compared to straight segments, vehicles often tend to be offset to one side when driving on curved segments. This is related to the turning position and the steering wheel angle. Understanding the offset trend of trajectories has reference value for improving road geometric design and setting safety facilities [43]. Based on this, we propose a parameterized trajectory classification method that employs the turning benefit ratio (TBR) and trajectory offset (Δd) as classification indicators for trajectories.

(1) Turning benefit ratio: The turning benefit ratio TBR as a classification indicator refers to the ratio of the trajectory's approximate radius to the ideal radius, as shown in equation (7). According to the coordinates of the starting point (x_s, y_s), midpoint (x_m, y_m), and endpoint (x_e, y_e) of the trajectory in the x-y coordinate system, the approximation radius R_T can be computed using Heron's formula [58], as shown in equation (8). According to TBR, we can classify trajectories into three patterns, as shown in Figure 5(a) When TBR ≈ 1, the vehicle trajectory radius is close to the ideal radius. In the Frenet coordinate system, the trajectory is then a straight line. (b) When TBR $\gg 1$, the trajectory radius is much larger than the ideal radius. In the Frenet coordinate system, the trajectory is a curve with the center on the right (the outer side of the curve). (c) When TBR $\ll 1$, the vehicle's trajectory radius is much smaller than the ideal radius. In the Frenet coordinate system, the trajectory is a curve with the center on the left (the inner side of the curve). Using the Frenet coordinate system provides an intuitive way to distinguish between three different trajectories classified by TBR.

$$\mathrm{TBR} = \frac{R_T}{R_C + d_B}, \tag{7}$$

$$\begin{cases} R_T = \dfrac{b_1 b_2 b_3}{4A}, \\ A = \sqrt{C(C-b_1)(C-b_2)(C-b_3)}, \\ C = \dfrac{b_1 + b_2 + b_3}{2}, \\ b_1 = \sqrt{(x_s - x_m) + (y_s - y_m)}, \\ b_2 = \sqrt{(x_m - x_e) + (y_m - y_e)}, \\ b_3 = \sqrt{(x_e - x_b) + (y_e - y_b)}, \end{cases} \tag{8}$$

where R_C is the radius of the road horizontal curve and d_B is the lateral distance between the vehicle and the road boundary when entering a curved segment.

(2) Trajectory offset distance: The trajectory offset Δd refers to the difference in lateral distance between the vehicle and the road boundary when entering and exiting a curved segment, i.e., $\Delta d = d_B - d_E$. Based on Δd, we can classify the trajectory into three categories, as shown in Figure 6. When $\Delta d \approx 0$, the

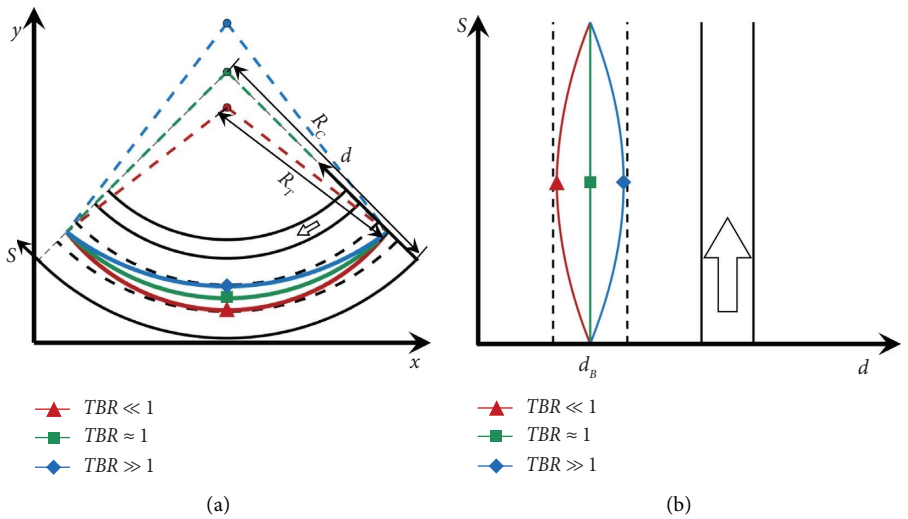

FIGURE 5: Schematic diagram of the vehicle trajectory with different TBR. In the Frenet coordinate system, the s-axis is located along the left boundary of the road, and the d-axis is perpendicular to the s-axis. The coordinate s represents the distance along the road, while the d-axis represents the vehicle's distance from the outer boundary. (a) Cartesian coordinates. (b) Frenet coordinates.

distance between the vehicle and the road boundary at the entry and exit of the curved segment is similar, indicating that the vehicle can maintain stable control. When $\Delta d \gg 0$, the vehicle deviates toward the outer side of the curve when exiting the curved segment. When $\Delta d \ll 0$, the vehicle deviates toward the inner side of the curve when exiting the curved segment. Although it is insufficient to determine insufficient or excessive steering solely based on trajectory offset, typically, when a vehicle has insufficient steering, it tends to deviate toward the outside of the curve. Conversely, when a vehicle has excessive steering, it tends to deviate toward the inside of the curve.

3.2.2. Trajectory Pattern Descriptions. To classify trajectories according to TBR and Δd, we introduce the standard deviation of two indicators, α and β, as deviation thresholds, respectively. When TBR $\in (1-\alpha, 1+\alpha)$, it can be considered that the approximation radius R_T of the trajectory is close to the ideal radius. When $\Delta d \in (-\beta, \beta)$, it can be considered that the distance between the vehicle and the road boundary is the same when the vehicle enters and exits the curved segment. In this study, vehicle trajectories are divided into nine patterns according to TBR and Δd, as shown in Figure 7.

The characteristics of the nine trajectory patterns are described as follows:

(1) Inside offset-smaller radius (I-S): This pattern has the characteristic that the trajectory's approximate radius R_T is much smaller than the ideal radius and deviates to the inside of the curve. Its $\Delta d \in (-\infty, -\beta]$ and TBR $\in (0, 1-\alpha]$. When the vehicle is oversteering, its trajectory may show this pattern.

(2) Inside offset-ideal radius (I-I): This pattern has the characteristic that the trajectory's approximate radius R_T is approximately equal to the ideal radius and deviates to the inside of the curve. Its $\Delta d \in (-\infty, -\beta]$ and TBR $\in (1-\alpha, 1+\alpha)$. This pattern is manifested as a straight line leaning towards the right side (the inner side of the curve) in the Frenet coordinate system.

(3) Inside offset-larger radius (I-L): This pattern has the characteristic that the trajectory's approximate radius R_T is much larger than the ideal radius and deviates to the inside of the curve. Its $\Delta d \in (-\infty, -\beta]$ and TBR $\in [1+\alpha, \infty)$. Unlike the "I-S" pattern, this pattern is infrequently encountered when the steering wheel angle remains constant. When the vehicle's trajectory displays this pattern, it signifies that the driver has made specific trajectory corrections.

(4) Symmetry-smaller radius (S-S): This pattern shows a symmetrical trajectory, but the trajectory's approximate radius R_T is much smaller than the ideal radius. Its $\Delta d \in (-\beta, \beta)$ and $TBR \in (0, 1-\alpha]$. This pattern may occur, but is not limited to situations when vehicles are compelled to adopt a smaller trajectory radius and offset towards the inner side to avoid intruding into the outermost lanes.

(5) Symmetry-ideal radius (S-I): This pattern shows a symmetrical trajectory with an approximate radius R_T is approximately equal to the ideal radius. Its $\Delta d \in (-\beta, \beta)$ and TBR $\in (1-\alpha, 1+\alpha)$. This is the ideal trajectory pattern, indicating that the vehicle can drive steadily along the geometric line of the lane. This pattern is manifested as a straight line parallel to the s-axis in the Frenet coordinate system.

(6) Symmetry-larger radius (S-L): This pattern shows a symmetrical trajectory, but the trajectory's

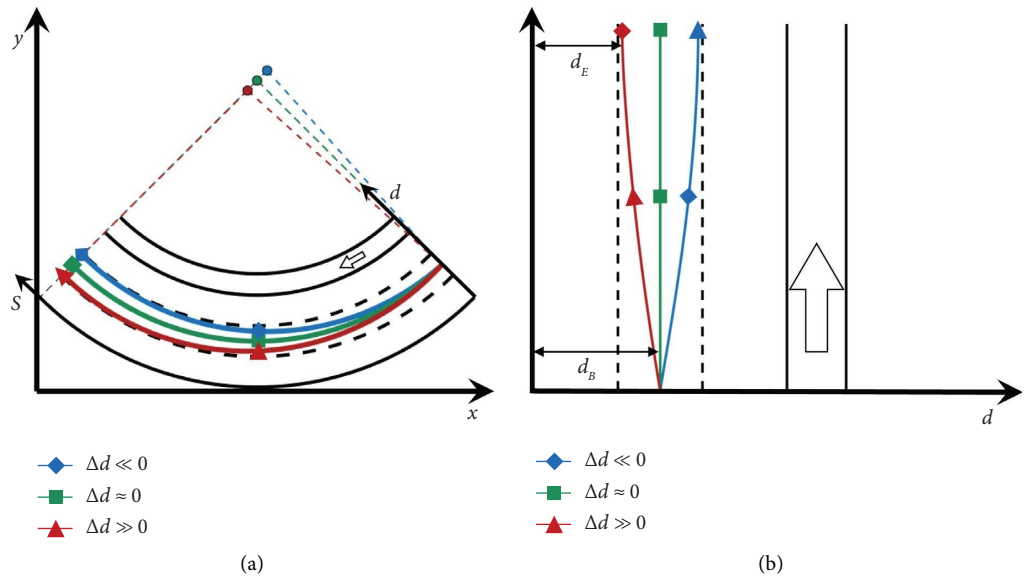

Figure 6: Schematic diagram of the vehicle trajectory with different Δd. (a) Cartesian coordinate. (b) Frenet coordinate.

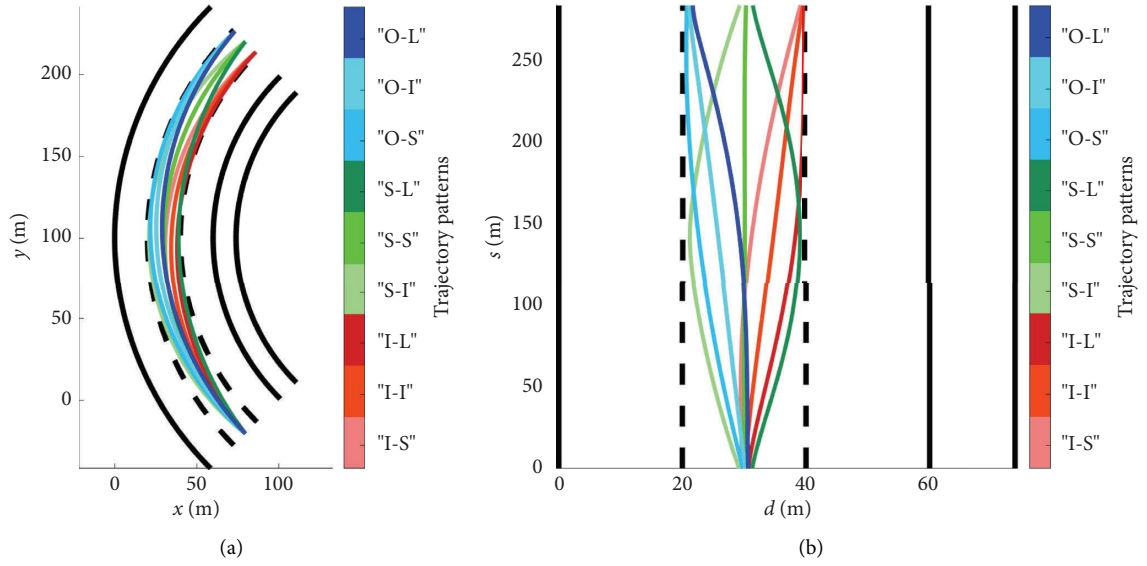

Figure 7: Schematic diagram of nine trajectory patterns. (a) Cartesian coordinate system. (b) Frenet coordinate system.

approximate radius R_T is much larger than the ideal radius. Its $\Delta d \in (-\beta, \beta)$ and TBR $\in [1+\alpha, \infty)$. When the vehicle is cutting to the inside of the curve, the vehicle's trajectory often exhibits this pattern.

(7) Outside offset-smaller radius (O-S): This pattern has the characteristic that the trajectory's approximate radius R_T is much smaller than the ideal radius and deviates to the outside of the curve. Its $\Delta d \in [\beta, \infty)$ and TBR $\in (0, 1-\alpha]$. Like the "I-L" pattern, this pattern is also infrequently encountered when the steering wheel angle remains constant. When the vehicle's trajectory displays this pattern, it signifies that the driver has made specific trajectory corrections.

(8) Outside offset-ideal radius (O-I): This pattern has the characteristic that the trajectory's approximate radius R_T is approximately equal to the ideal radius and deviates to the outside of the curve. Its $\Delta d \in [\beta, \infty)$ and TBR $\in (1-\alpha, 1+\alpha)$. This pattern is manifested as a straight line leaning towards the left side (the outer side of the curve) in the Frenet coordinate system.

(9) Outside offset-larger radius (O-L): This pattern has the characteristic that the trajectory's approximate radius R_T is much larger than the ideal radius and deviates to the outside of the curve. Its $\Delta d \in [\beta, \infty)$ and TBR $\in [1+\alpha, \infty)$. When the vehicle is understeering, its trajectory may show this pattern.

3.3. Sideslip Risk Measurement

3.3.1. Friction Coefficient Utilization Rate. Sideslip is the most common situation in lateral instability [59]. Figure 8 illustrates the forces acting on a vehicle on a curved segment during its travel. The vehicle experiences three primary forces in the lateral direction: the component of the vehicle's centrifugal force along the road's cross slope $F_v \cos\theta$, the component of the vehicle's gravitational force along the road's cross slope $G \sin\theta$, and the lateral resistance caused by the friction between the tires and the road surface F_f [60]. The centrifugal force is related to the vehicle's mass m, speed v, and trajectory radius R and can be represented as $F_v = mv^2/R$. When the vehicle is stable in the lateral direction, $F_v \cos\theta = G \sin\theta + F_f$. We define the required friction coefficient f_R for the vehicle to maintain lateral stability as the ratio of the lateral friction resistance F_f to the normal reaction force N. Accordingly, it can be known that f_R is related to the vehicle's instantaneous speed v_i, instantaneous turning radius R_i, and road cross slope e. The required friction coefficient f_R can be calculated according to equation (9). When the required friction coefficient f_R is less than the maximum friction coefficient $f_{\max}$ that can be provided between the tire and the road surface, the vehicle maintains lateral force balance.

$$f_R = \frac{{v_i}^2}{gR_i} - e \left(f_R \le f_{\max}\right). \tag{9}$$

When the required friction coefficient f_R for a vehicle is greater than the maximum friction coefficient $f_{\max}$ that the interaction between the tires and the road surface can provide, the vehicle will sideslip [61]. To enable a comprehensive comparison of the sideslip risk under clear and rainy weather conditions, we employ the friction coefficient utilization rate μ to measure the sideslip risk, as shown in equation (10). A higher value of μ translates to a greater risk of vehicle sideslip. However, it is difficult to obtain an accurate value for $f_{\max}$. Therefore, this study only selects the representative value of $f_{\max}$ under clear and rainy weather conditions for measuring the sideslip risk. According to related research [62], the maximum lateral friction coefficient for asphalt surfaces is approximately 0.85 under clear weather conditions and approximately 0.30 under rainy conditions.

$$\mu = \frac{\max\{f_R\}}{f_{\max}}. \tag{10}$$

3.3.2. Data Extraction and Optimization. Speed $\{v_i\}$ and trajectory radius $\{R_i\}$ of the vehicle are critical basic data for measuring vehicle sideslip risk. They can be calculated based on the trajectory coordinates in the x-y coordinate system using equations (11) and (12), respectively. Here, the x and y coordinates are respectively fitted using fourth-degree polynomials to obtain the first and second derivatives.

$$\{R_i\} = \frac{1}{\{k_i\}} = \left|\frac{\left(x'^2 + y'^2\right)^{3/2}}{x'y'' - x''y'}\right|, \tag{11}$$

$$\{v_i\} = \sqrt{x'^2 + y'^2}, \tag{12}$$

where $\{k_i\}$ is the curvature at each trajectory point.

Due to the random noise introduced during trajectory extraction processing steps, this study chose filtering techniques to optimize the data. Filtering is a data processing technique used to remove noise and enhance the accuracy of information extraction [63]. Commonly used algorithms include median and mean filters, wavelet thresholding, a cubic spline filter, and a Savitzky–Golay filter [64]. Compared to other algorithms, the Savitzky–Golay filter has the advantage of preserving data features and allowing for flexible parameter adjustment. Moreover, it has been found effective for optimizing vehicle trajectory data [65]. The Savitzky–Golay filter is given in the following equation:

$$Q_j = \frac{\sum_{i=-m}^{i=m} \lambda_i q_{j+1}}{N}, \tag{13}$$

where Q_j is the filtered data; q_{j+1} is the original data; λ_i is the i-th coefficient of the filter, which can be calculated by a polynomial with order ω; N is the filter length; and m is the half-filter length, which is equal to $0.5(N-1)$.

4. Data Preparation and Implementation Details

The data for this study originate from the S4 highway in China, a major arterial route with three lanes in each direction and a design speed of 120 km/h. According to the crash report, we selected a curved segment with six rainy sideslip crashes in two years as the study segment. This segment has a curvature radius of 2,200 m and a superelevation of 3%. The data collected comprise surveillance video and highway design drawings. Two surveillance videos were used as case studies, which were recorded in different weather conditions: clear and rainy weather (as shown in Figure 9). The videos were captured using gun-type surveillance cameras fitted with rain shields to ensure quality recording in rainy conditions. Each video boasts a resolution of 4,064 pixels × 3,040 pixels and a frame rate of 24 frames/second, spanning a duration of two hours. The traffic volume in both videos is approximately equivalent, recording 970 vehicles under clear weather conditions and 1,021 vehicles during rainy conditions.

Vehicle types are classified into two categories: "Car" and "Truck." "Car" refers to vehicles with no more than two axles or four wheels (e.g., private cars and vans), while "Truck" refers to vehicles with more than two axles or four wheels (e.g., trucks and buses). Meanwhile, road lanes are divided into left, middle, and right lanes according to the direction of vehicle travel. The left lane is closer to the outside of the curve, and the right lane is closer to the inside of the curve.

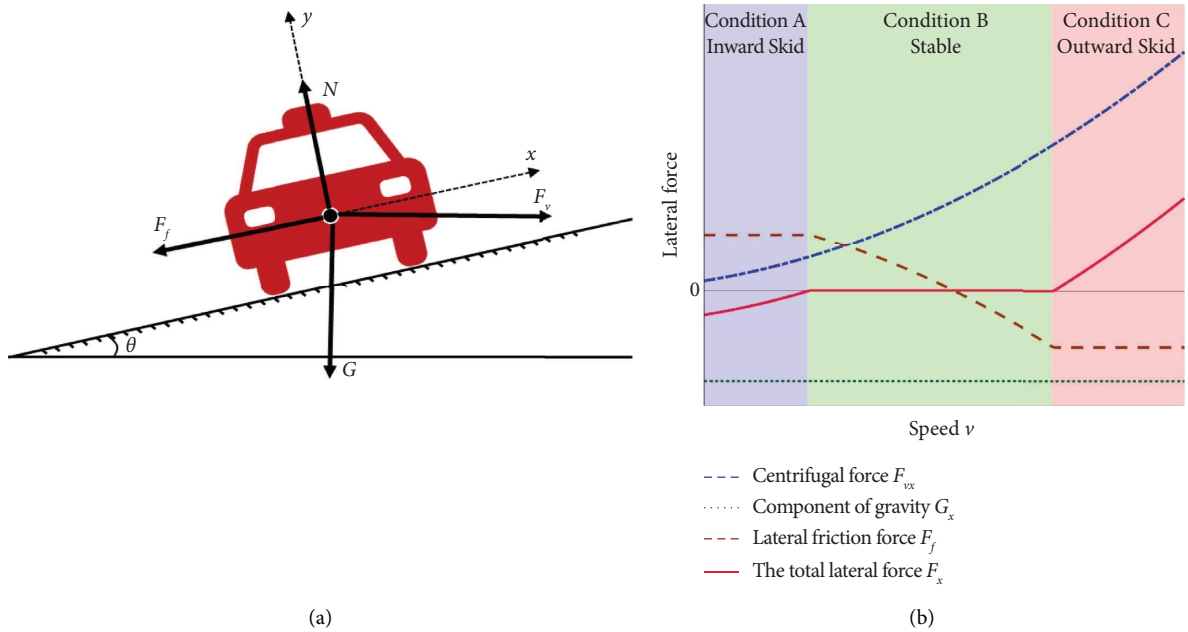

FIGURE 8: Front view of vehicle model on a curved segment. (a) Lateral force of the vehicle on the curved segment. (b) Vehicle lateral stability at different speed.

The vehicle's lane is identified based on the lane it occupied when entering the segment, as shown in Figure 9(a).

In addition, we calibrated the parameters of the camera that captured these surveillance videos using the method described in Section 3.1.2. Based on the road markings, we located a vanishing point with coordinates $(u_0, v_0) = (676.99, -102.14)$. Further, utilizing the known information from the image, a lane width of 3.75 m and a road marking length of 6.00 m, we applied equations (2)–(6) to calculate the camera's rotation angle $\sigma = 0.027$, the pitch angle $\phi = 0.062$, the focal length $f = 10296.18$, and the camera height $h = 8.99m$. Based on this, we further defined the effective trajectory observation area and determined the grid mesh using equation (1), as shown in Figure 9(b).

5. Results and Discussion

5.1. Trajectory Pattern Statistical Analysis. This section primarily includes two aspects: (a) conducting statistical analysis on two trajectory classification indicators to determine the classification threshold and (b) exploring the influence of vehicle lane and vehicle type on trajectory patterns in different weather conditions.

5.1.1. Classification Indicators and Deviation Thresholds. In order to classify trajectories according to the two indicators TBR and Δd proposed in this study, it is necessary to determine the deviation thresholds α and β. We performed a statistical analysis on TBR and Δd under clear and rainy weather conditions. Table 2 presents the statistical results, including the mean, standard deviation, skewness, and kurtosis of TBR and Δd.

According to Table 2, we can conduct a preliminary analysis of the impact of rainfall on the trajectory. It can be observed that rainy weather increases the mean and skewness of both TBR and Δd when compared to clear weather. This suggests that vehicles tend to deviate towards the outside of curves and adopt a larger trajectory radius on curved segments under rainy weather. Furthermore, rainy weather causes a decrease in the kurtosis of Δd and an increase in its standard deviation when compared to clear weather conditions. It also suggests that the offset dispersion is greater as the vehicle crosses the curved segment under rainy conditions. Notably, rainy conditions also reduce the kurtosis and the standard deviation of TBR compared to clear weather conditions. This suggests that, under rainy conditions, the trajectory approximation radius R_T dispersion increases within a limited range while extreme deviations decrease.

Considering that the trajectories collected under clear weather are more representative of the normal situation, this study chooses the standard deviations of two indicators as deviation thresholds: $\alpha = 0.093$ and $\beta = 0.685$. The collected vehicle trajectories are classified into nine patterns using these thresholds. Figure 10 presents the classification results of the trajectory under rainy weather conditions, clearly illustrating the significant characteristics differences among the nine patterns. These characteristics of the nine trajectory patterns are consistent with the features described in Section 3.2.2. This result validates the feasibility and effectiveness of the trajectory pattern classification method combined with computer vision technology proposed in this study.

5.1.2. Exploratory Analysis of Trajectory Pattern. Based on the classification of trajectory patterns, we investigate the influence of rainfall on trajectory patterns for vehicles with different vehicle types and lanes. Table 3 displays the

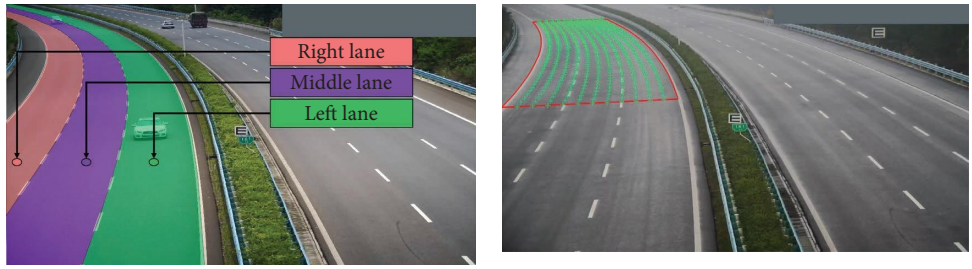

(a) (b)

Figure 9: Surveillance video screenshots of study segment in different weather conditions. (a) Video screenshots under clear weather condition with lane location indication. (b) Video screenshots under rainy weather condition with grid mesh indication.

Table 2: Statistical analysis of trajectory classification indicators.

Weather	Number of samples	Mean		Standard deviation		Skewness		Kurtosis	
		TBR	Δd	TBR	Δd	TBR	Δd	TBR	Δd
Clear	970	1.032	0.147	0.093	0.685	0.362	−0.190	6.729	15.051
Rainy	1021	1.035	0.295	0.084	0.743	0.624	0.449	5.991	8.172

proportions of different trajectory patterns under clear and rainy weather conditions across various lanes. The following observations are noteworthy:

(a) Under rainy conditions, the proportion of the "S-I" trajectory pattern (the theoretically ideal trajectory pattern) decreases in all three lanes. This suggests that rainfall may heighten the challenge of controlling the vehicle along the geometric path of the road on curved segments.

(b) Compared to clear weather conditions, the proportion of vehicles in the left lane that deviates to the outside (left side) of the curve increases significantly under rainy conditions, while the proportion of vehicles in the right lane that deviates to the inside (right side) of the curve increases slightly. Among them, the "O-I" trajectory pattern increases by 25% in the left lane, while the "I-I" trajectory pattern increases by 7.4% in the right lane. This finding implies that vehicles on the left and right lanes may tend to stay away from the middle lane under rainy conditions.

(c) Vehicles adopting the "S-L" trajectory pattern must shift towards the middle lane when in the left lane, whereas vehicles in the right lane must deviate from the middle lane. Compared to clear weather conditions, the proportion of the "S-L" trajectory pattern decreases by 4.8% in the left lane, while it increases by 4.3% in the right lane. This finding supports the speculation that vehicles on the left and right lanes may tend to stay away from the middle lane under rainy conditions.

(d) In the middle lane, aside from a 7.8% reduction in the proportion of the "S-I" pattern, changes in other trajectory patterns remain below 3%. This indicates that the vehicle trajectory pattern in the middle lane is least affected by rainfall.

Table 4 illustrates the proportions of different trajectory patterns for various vehicle types under clear and rainy weather conditions. The following trends can be observed:

(a) Compared to clear weather conditions, the proportion of the "S-I" trajectory pattern for cars decreases by 14.5%, while for trucks, it only decreases by 6.9%. This suggests that car trajectory patterns may be more susceptible to rainfall compared to trucks.

(b) Compared to clear weather conditions, under rainy conditions, the proportion of the "O-I" trajectory pattern for cars and trucks shows a substantial increase of 12.3% and 6.2%, respectively. Meanwhile, the proportion of trucks with the "I-L" trajectory pattern decreases by 4.8% under rainy days, and the "O-L" trajectory pattern increases by 4.2%. This may indicate a tendency for vehicles to deviate towards the outside of curved segments.

5.2. Sideslip Risk Analysis. This section focuses on two aspects: (a) analyzing the influence of rainfall on speed and the minimum curvature radius of trajectories and measuring the sideslip risk in different weather conditions and (b) comparing and analyzing the sideslip risk associated with different trajectory patterns.

5.2.1. Analysis of the Impact of Rainfall. A vehicle's speed and turning radius are key factors that influence the risk of a sideslip. Figure 11 illustrates the relationship between speed and trajectory curvature radius under clear and rainy

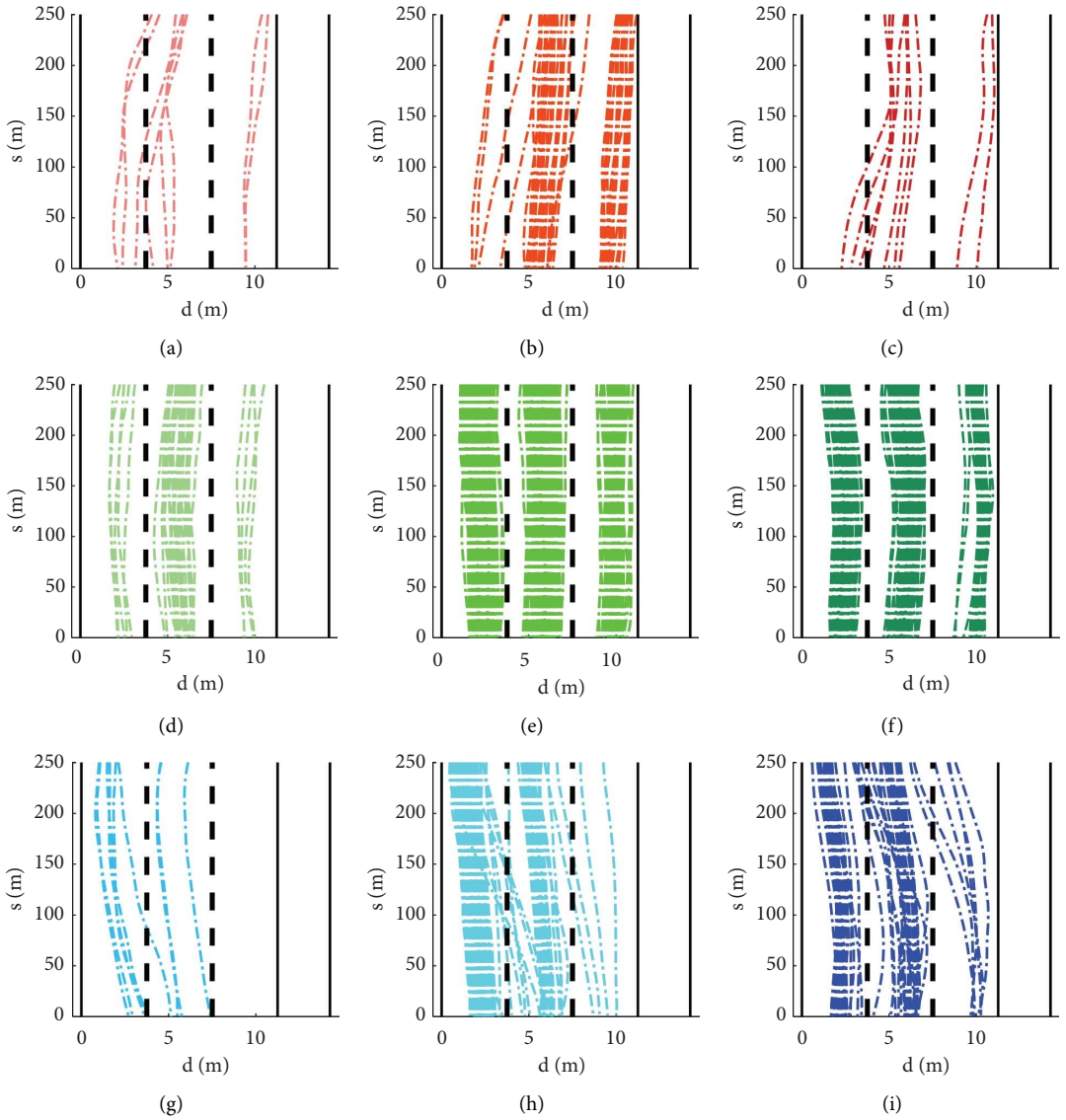

Figure 10: Trajectory classification results of datasets from the rainy case. (a) "I-S" pattern ($n = 8$). (b) "I-I" pattern ($n = 44$). (c) "I-L" pattern ($n = 9$). (d) "S-S" pattern ($n = 32$). (e) "S-I" pattern ($n = 555$). (f) "S-L" pattern ($n = 136$). (g) "O-S" pattern ($n = 9$). (h) "O-I" pattern ($n = 172$). (i) "O-L" pattern ($n = 56$).

Table 3: Distribution of trajectory patterns across different lanes and weather conditions (%).

Lane	Weather	I-S	I-I	I-L	S-S	S-I	S-L	O-S	O-I	O-L
Left lane	Clear ($n = 340$)	0.000	0.000	0.000	0.000	67.647	14.706	1.471	8.824	7.353
	Rainy ($n = 404$)	0.000	0.248	0.000	1.238	46.535	9.901	1.485	33.911	6.683
Change		0.000	+0.248	0.000	+1.238	**−21.112**	**−4.805**	+0.015	**+25.087**	−0.670
Middle lane	Clear ($n = 530$)	0.000	3.774	1.887	5.660	68.868	13.208	0.000	3.774	2.830
	Rainy ($n = 508$)	1.181	4.724	1.378	4.528	61.024	14.764	0.591	6.693	5.118
Change		+1.181	+0.951	−0.509	−1.133	**−7.844**	+1.556	+0.591	+2.919	+2.288
Right lane	Clear ($n = 100$)	5.000	10.000	5.000	0.000	65.000	15.000	0.000	0.000	0.000
	Rainy ($n = 109$)	1.835	17.431	1.835	3.670	52.294	19.266	0.000	0.917	2.752
Change		−3.165	**+7.431**	−3.165	+3.670	**−12.706**	**+4.266**	0.000	+0.917	+2.752

Note. n is the number of vehicles. Other values are in percent. The data in bold mean that the change value is greater than 4%.

Table 4: Distribution of trajectory patterns across vehicle types and weather conditions (%).

Type	Weather	I-S	I-I	I-L	S-S	S-I	S-L	O-S	O-I	O-L
Car	Clear ($n = 865$)	0.578	2.890	1.156	3.468	68.786	13.295	0.578	5.202	4.046
	Rainy ($n = 921$)	0.869	4.560	0.977	3.257	54.289	12.595	0.869	17.481	5.103
Change		+0.291	+1.670	−0.179	−0.211	**−14.497**	−0.700	+0.291	**+12.279**	+1.057
Truck	Clear ($n = 105$)	0.000	4.762	4.762	0.000	61.905	19.048	0.000	4.762	4.762
	Rainy ($n = 100$)	0.000	2.000	0.000	2.000	55.000	20.000	1.000	11.000	9.000
Change		0.000	−2.762	**−4.762**	+2.000	**−6.905**	+0.952	+1.000	**+6.238**	**+4.238**

Note. n is the number of vehicles. Other values are in percent. The data in bold mean that the change value is greater than 4%.

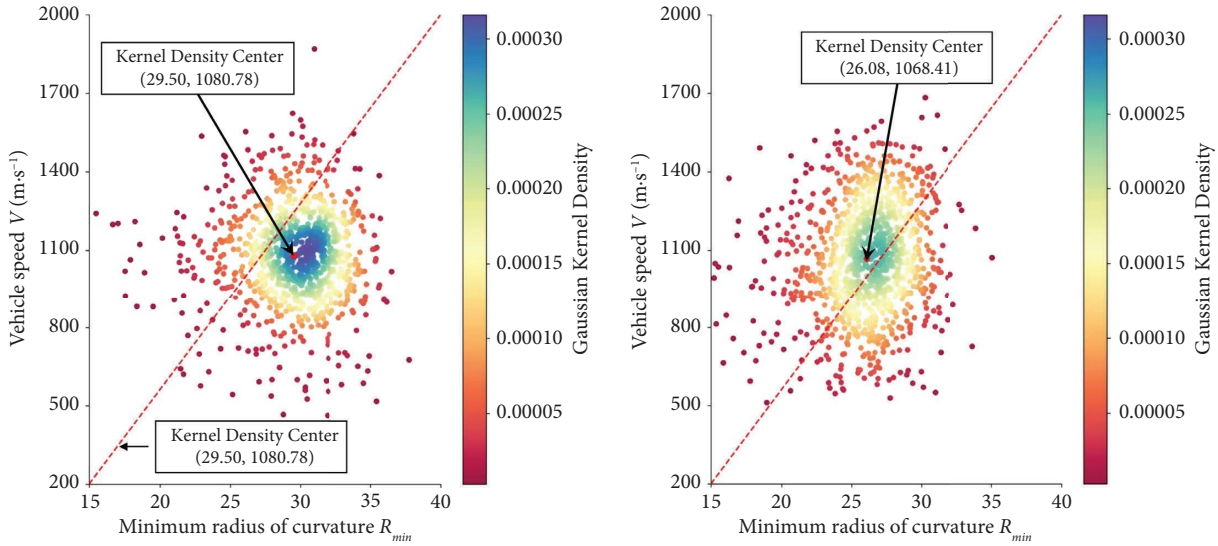

Figure 11: Comparative scatter distributions of vehicle speed and minimum curvature radius under clear and rainy weather conditions. The red dashed line in the figures is the diagonal line of the coordinate axis, which is convenient for observing the changes. (a) Clear weather condition. (b) Rainy weather condition.

weather conditions. Each data point represents a vehicle, where the y-axis represents the minimum curvature radius $R_{\min}$ of the vehicle's trajectory on curved segments, and the x-axis represents the corresponding vehicle speed at that moment. The color of each scatter point represents the density at its corresponding position, indicating the number of points in that location. This density is obtained through Gaussian kernel density estimation. Several trends can be observed from this figure:

(a) Under rainy weather conditions, the average vehicle speed significantly decreases (29.50 m/s for clear weather conditions, 26.08 m/s for rainy weather conditions). This confirms that rainfall has a significant impact on drivers.

(b) Under rainy weather conditions, the mean value of $R_{\min}$ decreases and its dispersion increases. This trend could indicate that drivers are more cautious or that rainfall may increase the difficulty for drivers to control their vehicles, consequently making it challenging for vehicles to adopt a larger trajectory radius when negotiating curves.

(c) Although there is no apparent linear relationship between vehicle speed and the minimum curvature radius ($R_{\min}$), there is a decreasing trend in vehicle speed with decreasing $R_{\min}$ under rainy weather conditions. In contrast, no such trend is observed under clear weather conditions. This trend may be related to the lateral stability of vehicles. In clear weather, the road surface offers higher skid resistance, and the vehicle is more laterally stable. However, in rainy conditions, with lower skid resistance, drivers may distinctly feel the risk of vehicle sideslip, especially when taking curves with smaller radius. As the risk of sideslip increases with smaller trajectory radius, drivers need to reduce speed to ensure the safe passage of the vehicle.

Figure 12 presents the distribution of the friction coefficient utilization rate μ under clear and rainy weather conditions. Under clear weather, the mean value of μ is 0.066

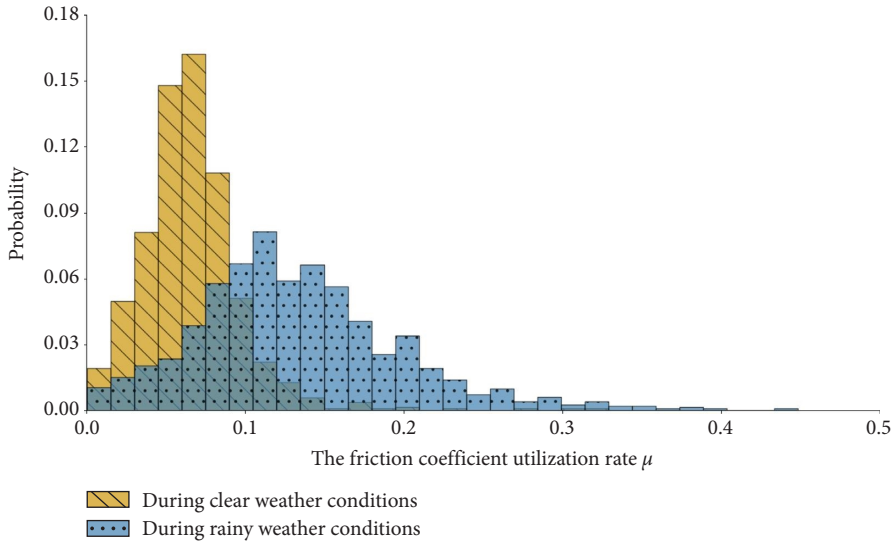

Figure 12: Comparative analysis of the friction coefficient utilization rate under clear and rainy weather conditions.

with a standard deviation of 0.032, whereas, under rainy conditions, the mean value of μ is 0.128 with a standard deviation of 0.068. Overall, there is a significant increase in μ for vehicles on curved segments under rainy conditions compared to clear weather conditions. Furthermore, the maximum value of μ under clear weather is 0.299, corresponding to a maximum required friction coefficient f_R of 0.255. In contrast, the maximum μ under rainy conditions reaches 0.493, corresponding to a maximum f_R of 0.148. Previous studies suggest that the maximum achievable coefficient of friction between tires and road surfaces under rainy conditions may be lower than 0.1 [66], indicating an elevated sideslip risk on such road segments under rainy conditions.

5.2.2. Analysis of Different Trajectory Patterns. Figure 13 illustrates the friction coefficient utilization rate μ of different trajectory patterns under clear and rainy weather conditions. Due to the limited sample size for some trajectory patterns, the median values may not be representative. Therefore, this study primarily uses the mean of μ to measure the sideslip risk of various trajectory patterns. The investigation reveals the following findings:

(a) Rainfall impacts sideslip risk differently for various trajectory patterns. Although the trajectory pattern with the highest risk of sideslip is "O-S" under both clear and rainy conditions, the trajectory pattern with the lowest risk of sideslip is different. The "S-L" trajectory pattern has the lowest sideslip risk under clear conditions. However, the "S-I" trajectory pattern has the lowest risk of sideslip under rainy conditions.

(b) Among the trajectory patterns of the same category based on TBR classification, there is no significant correlation between Δd and the mean of μ under clear weather conditions. However, under rainy conditions, the symmetrical trajectory patterns ("S-S," "S-I," and "S-L") exhibit a lower mean of μ. This finding indicates that maintaining a constant lateral distance from the lane under rainy conditions can reduce the vehicle's sideslip risk.

(c) Among the trajectory patterns of the same category based on Δd classification, the mean value of μ for varying patterns displays a certain order under clear weather conditions: smaller radius > ideal radius > larger radius. However, under rainy conditions, the mean value of μ for different trajectory patterns follows this order: smaller radius > larger radius > ideal radius. It can be seen that there is a certain correlation between the μ of the vehicle and the TBR of the trajectory. The trajectory pattern with smaller TBR exhibits a higher risk of sideslip under clear weather conditions. However, this correlation is not observed under rainy conditions. Under rainy conditions, there is a tendency for the TBR of a trajectory to be closer to 1.00, which lowers its sideslip risk. This finding reveals that adopting a larger TBR under rainy conditions does not necessarily reduce vehicle sideslip risk. Conversely, this may increase the sideslip risk when using the "S-L," "I-L," and "O-L" trajectory patterns.

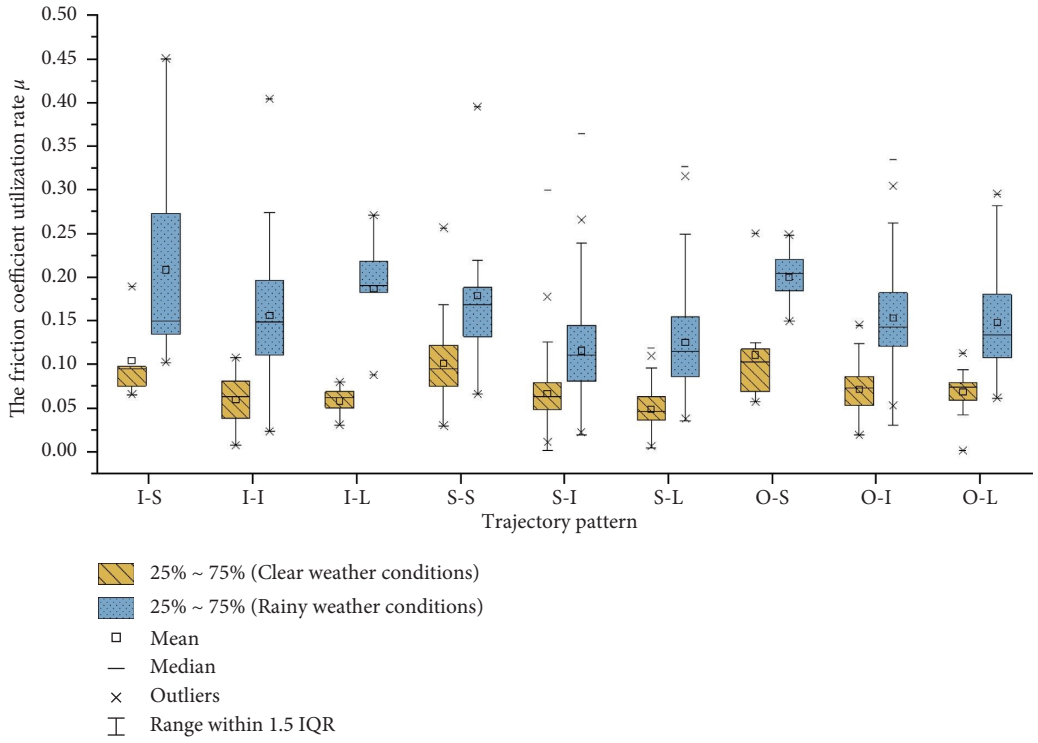

Figure 13: Comparative analysis of the friction coefficient utilization rate in different trajectory patterns.

6. Conclusion

To sum up, this study aimed to investigate the influence of rainfall on trajectory patterns and sideslip risk on highway curves. The main contributions of this study are as follows. Firstly, the turning benefit ratio TBR and trajectory offset Δd were introduced as parameterized classification indicators for trajectories, addressing the lack of precise indicators for systematic trajectory classification on curved segments. Furthermore, the friction coefficient utilization rate μ was adopted as a measure for sideslip risk. Secondly, we proposed a computer vision-based framework for automatically identifying trajectory patterns and measuring sideslip risk. Using this approach, we collected the trajectories and their sideslip risk data from a curved segment of highway in China under clear and rainy weather conditions. Based on the data, a case study was conducted, and the following important conclusions were drawn:

(a) According to the proposed trajectory classification indicators, the turning benefit ratio TBR, and trajectory offset Δd, vehicle trajectories can be effectively classified into nine patterns using computer vision techniques. Meanwhile, in the Frenet coordinate system, these nine trajectory patterns show significant characteristic differences, which is helpful for better observation of trajectory changes. This classification method provides traffic management authorities with an effective tool for more accurate and parameterized monitoring of vehicle behaviors and sideslip risks on highways, especially during rainy weather conditions.

(b) The impact of rainfall on trajectory patterns of vehicles in different lanes, ranked in descending order, is as follows: left lane (outer side of the curve) > right lane (inner side of the curve) > middle lane. Meanwhile, cars are more susceptible to these impacts compared to trucks. In addition, compared to clear weather conditions, vehicles on the left and right lanes may tend to stay away from the middle lane under rainy conditions. This finding directs traffic management authorities towards prioritizing certain lanes for management and aids highway designers in improving road design to accommodate these observed behaviors.

(c) Rainfall significantly increased the sideslip risk on the curved segments. However, the influence of rainfall on sideslip risk varied among different trajectory patterns. Under rainy conditions, both the trajectory's approximation radius and the offset have a significant impact on the sideslip risk. The "S-I" trajectory pattern has the lowest risk of sideslip under rainy conditions. Symmetrical trajectory patterns are safer than asymmetrical patterns, and trajectories closer to the ideal radius are safer than others. Thus, maintaining a steady lateral distance under rainy conditions can contribute to avoiding vehicle sideslip. This finding could help develop or improve advanced driver assistance systems (ADAS)

that can automatically adjust a vehicle's trajectory in rainy weather to reduce the sideslip risk.

However, there are some limitations to this study. It only compares the changes in trajectory patterns under different weather conditions on the same road segment, without considering the sensitivity of road trajectories to rainfall at different radii. In addition, the study lacks actual measurements of lateral friction coefficients on the road surface, comparing only the relative relationships of sideslip risks among different trajectories. Future work aims to collect more research data and further investigate the impact of factors such as road radius and longitudinal slope on trajectory patterns, providing a clearer understanding of the effects of rainfall on vehicle safety on curved segments.

Data Availability

The authors do not have permission to share data.

Conflicts of Interest

The authors declare that there are no conflicts of interest.

Acknowledgments

A fair amount of the research works is conducted at the Nanyang Technological University Singapore to which the first author was attached as a visiting PhD candidate sponsored by the China Scholarship Council. This work was supported by the Key Technologies Research and Development Program of China (Grant No. 2020YFC1512005), the Key Research and Development Program of Sichuan Province (Grant No. 2022YFG0048), the Key Research and Development Program of Shanxi Province (Grant No. 202102020101014), and the Science and Technology Project of Sichuan Transportation Department (Grant Nos. 2019-ZL-12 and 2022-ZL-04).

References

[1] E. M. Ali, M. M. Ahmed, and S. S. Wulff, "Detection of critical safety events on freeways in clear and rainy weather using SHRP2 naturalistic driving data: parametric and non-parametric techniques," *Safety Science*, vol. 119, pp. 141–149, 2019.

[2] M. Yan, J. Xu, S. Han et al., "Permitted speed decision of single-unit trucks with emergency braking maneuver on horizontal curves under rainy weather," *PLoS One*, vol. 16, no. 12, Article ID e0261975, 2021.

[3] S. E. Stevens, C. J. Schreck, S. Saha, J. E. Bell, and K. E. Kunkel, "Precipitation and fatal motor vehicle crashes: continental analysis with high-resolution radar data," *Bulletin of the American Meteorological Society*, vol. 100, no. 8, pp. 1453–1461, 2019.

[4] S. Das, A. Dutta, and X. Sun, "Patterns of rainy weather crashes: applying rules mining," *Journal of Transportation Safety & Security*, vol. 12, no. 9, pp. 1083–1105, 2019.

[5] P. Li and J. He, "Geometric design safety estimation based on tire–road side friction," *Transportation Research Part C: Emerging Technologies*, vol. 63, pp. 114–125, 2016.

[6] C. Caliendo, M. Guida, and A. Parisi, "A crash-prediction model for multilane roads," *Accident Analysis & Prevention*, vol. 39, no. 4, pp. 657–670, 2007.

[7] X. Wang, H. Q. Pu, X. Li, Y. Yan, and J. Yao, "A new GNB model of crash frequency for freeway sharp horizontal curve based on interactive influence of explanatory variables," *Journal of Advanced Transportation*, vol. 2018, Article ID 8973581, 9 pages, 2018.

[8] S. Kim, J. Lee, and T. Yoon, "Road surface conditions forecasting in rainy weather using artificial neural networks," *Safety Science*, vol. 140, Article ID 105302, 2021.

[9] Y. D. Wong and A. Nicholson, "Driver behaviour at horizontal curves: risk compensation and the margin of safety," *Accident Analysis & Prevention*, vol. 24, no. 4, pp. 425–436, 1992.

[10] F. Rosey and J. M. Auberlet, "Trajectory variability: road geometry difficulty indicator," *Safety Science*, vol. 50, no. 9, pp. 1818–1828, 2012.

[11] X. Liu, Q. Cao, H. Wang, J. Chen, and X. Huang, "Evaluation of vehicle braking performance on wet pavement surface using an integrated tire-vehicle modeling approach," *Transportation Research Record: Journal of the Transportation Research Board*, vol. 2673, no. 3, pp. 295–307, 2019.

[12] J. Lee, J. Chae, T. Yoon, and H. Yang, "Traffic accident severity analysis with rain-related factors using structural equation modeling – a case study of Seoul City," *Accident Analysis & Prevention*, vol. 112, pp. 1–10, 2018.

[13] S. Lee, J. Choi, and S. W. Kim, "Bayesian approach with the power prior for road safety analysis," *Transportmetrica*, vol. 6, no. 1, pp. 39–51, 2010.

[14] Q. Hou, X. Huo, J. Leng, and Y. Cheng, "Examination of driver injury severity in freeway single-vehicle crashes using a mixed logit model with heterogeneity-in-means," *Physica A: Statistical Mechanics and its Applications*, vol. 531, Article ID 121760, 2019.

[15] G. Tian, Y. Jia, Z. Chen et al., "Evaluation on lateral stability of vehicle: impacts of pavement rutting, road alignment, and adverse weather," *Applied Sciences*, vol. 13, no. 5, p. 3250, 2023.

[16] T. Peng, L. L. Su, Z. W. Guan et al., "Lane-change model and tracking control for autonomous vehicles on curved highway sections in rainy weather," *Journal of Advanced Transportation*, vol. 2020, Article ID 8838878, 15 pages, 2020.

[17] A. Theofilatos and G. Yannis, "A review of the effect of traffic and weather characteristics on road safety," *Accident Analysis & Prevention*, vol. 72, pp. 244–256, 2014.

[18] A. Ghasemzadeh and M. M. Ahmed, "Utilizing naturalistic driving data for in-depth analysis of driver lane-keeping behavior in rain: non-parametric MARS and parametric logistic regression modeling approaches," *Transportation Research Part C: Emerging Technologies*, vol. 90, pp. 379–392, 2018.

[19] S. Chen, L. Piao, X. Zang et al., "Analyzing differences of highway lane-changing behavior using vehicle trajectory data," *Physica A: Statistical Mechanics and its Applications*, vol. 624, Article ID 128980, 2023.

[20] A. Das and M. M. Ahmed, "Adjustment of key lane change parameters to develop microsimulation models for representative assessment of safety and operational impacts of adverse weather using SHRP2 naturalistic driving data," *Journal of Safety Research*, vol. 81, pp. 9–20, 2022.

[21] R. S. Sakhare, Y. Zhang, H. Li, and D. M. Bullock, "Impact of rain intensity on interstate traffic speeds using connected vehicle data," *Vehicles*, vol. 5, no. 1, pp. 133–155, 2023.

[22] E. M. Ali, M. M. Ahmed, and G. Yang, "Normal and risky driving patterns identification in clear and rainy weather on freeway segments using vehicle kinematics trajectories and time series cluster analysis," *IATSS Research*, vol. 45, no. 1, pp. 137–152, 2021.

[23] A. Das, M. N. Khan, M. M. Ahmed, and S. S. Wulff, "Cluster analysis and multi-level modeling for evaluating the impact of rain on aggressive lane-changing characteristics utilizing naturalistic driving data," *Journal of Transportation Safety & Security*, vol. 14, no. 12, pp. 2137–2165, 2022.

[24] O. Lappi, "Future path and tangent point models in the visual control of locomotion in curve driving," *Journal of Vision*, vol. 14, no. 12, p. 21, 2014.

[25] Y. Chen, M. Quddus, and X. Wang, "Impact of combined alignments on lane departure: a simulator study for mountainous freeways," *Transportation Research Part C: Emerging Technologies*, vol. 86, pp. 346–359, 2018.

[26] Z. Yu, Y. Chen, X. Zhang, and J. Xu, "Track behavior and crash risk analysis of passenger cars on hairpin curves of two-lane mountain roads," *Journal of Advanced Transportation*, vol. 2021, Article ID 4906360, 15 pages, 2021.

[27] P. Spacek, "Track behavior in curve areas: attempt at typology," *Journal of Transportation Engineering*, vol. 131, no. 9, pp. 669–676, 2005.

[28] X. Kuang and Z. Chen, "Trajectory research of Cellular Automaton Model based on real driving behaviour," *Physica A: Statistical Mechanics and its Applications*, vol. 602, Article ID 127610, 2022.

[29] J. Song, Y. Fan, H. Song, and H. Zhao, "Target tracking and 3D trajectory reconstruction based on multicamera calibration," *Journal of Advanced Transportation*, vol. 2022, Article ID 5006347, 8 pages, 2022.

[30] X. Tang, Z. Zhang, and Y. Qin, "On-road object detection and tracking based on radar and vision fusion: a review," *IEEE Intelligent Transportation Systems Magazine*, vol. 14, no. 5, pp. 103–128, 2022.

[31] T. Xu, Z. Zhang, X. Wu, L. Qi, and Y. Han, "Recognition of lane-changing behaviour with machine learning methods at freeway off-ramps," *Physica A: Statistical Mechanics and its Applications*, vol. 567, Article ID 125691, 2021.

[32] N. Raju, S. Arkatkar, and C. Antoniou, "Investigating traffic safety reckoning hyperbolic driving following behavior using trajectory data," *Physica A: Statistical Mechanics and its Applications*, vol. 606, Article ID 128129, 2022.

[33] D. Selmanaj, M. Corno, G. Panzani, and S. M. Savaresi, "Vehicle sideslip estimation: a kinematic based approach," *Control Engineering Practice*, vol. 67, pp. 1–12, 2017.

[34] H. F. Grip, L. Imsland, T. A. Johansen, J. C. Kalkkuhl, and A. Suissa, "Vehicle sideslip estimation: design, implementation, and experimental validation," *IEEE Control Systems*, vol. 29, pp. 36–52, 2009.

[35] D. Chindamo, B. Lenzo, and M. Gadola, "On the vehicle sideslip angle estimation: a literature review of methods, models, and innovations," *Applied Sciences*, vol. 8, no. 3, p. 355, 2018.

[36] W. Chen, D. Tan, and L. Zhao, "Vehicle sideslip angle and road friction estimation using online gradient descent algorithm," *IEEE Transactions on Vehicular Technology*, vol. 67, no. 12, pp. 11475–11485, 2018.

[37] J. H. Yoon, S. Eben Li, and C. Ahn, "Estimation of vehicle sideslip angle and tire-road friction coefficient based on magnetometer with GPS," *International Journal of Automotive Technology*, vol. 17, no. 3, pp. 427–435, 2016.

[38] M. Yu, Z. You, G. Wu, L. Kong, C. Liu, and J. Gao, "Measurement and modeling of skid resistance of asphalt pavement: a review," *Construction and Building Materials*, vol. 260, Article ID 119878, 2020.

[39] American Association of State Highway and Transportation Officials, *A Policy on Geometric Design of Highways and Streets*, American Association of State Highway and Transportation Officials, Washington, DC, USA, 2018.

[40] B. Wang, C. Zhang, M. Zhang, C. Liu, Z. Xie, and H. Zhang, "Digital twin analysis for driving risks based on virtual physical simulation technology," *IEEE Journal of Radio Frequency Identification*, vol. 6, pp. 938–942, 2022.

[41] C. Sun, C. Wu, D. Chu, M. Zhong, Z. Hu, and J. Ma, "Risk prediction for curve speed warning by considering human, vehicle, and road factors," *Transportation Research Record*, vol. 2581, pp. 18–26, 2016.

[42] S. Tian, X. Luo, C. Xiao, and J. Zhou, "Rail vehicle running safety and steering efficiency evaluation method based on equivalent curvature difference of active steering technology," *Vehicle System Dynamics*, vol. 61, no. 5, pp. 1189–1209, 2022.

[43] J. Xu, X. Luo, and Y. M. Shao, "Vehicle trajectory at curved sections of two-lane mountain roads: a field study under natural driving conditions," *European Transport Research Review*, vol. 10, pp. 12–16, 2018.

[44] F. Mauriello, A. Montella, M. Pernetti, and F. Galante, "An exploratory analysis of curve trajectories on two-lane rural highways," *Sustainability*, vol. 10, no. 11, p. 4248, 2018.

[45] R. Yuan-yuan, L. Xian-sheng, R. You, R. Guan, and G. Wei-wei, "Study on driving dangerous area in road curved section based on vehicle track characteristics," *International Journal of Computational Intelligence Systems*, vol. 4, no. 6, pp. 1237–1245, 2011.

[46] M. E. S. Rondora, A. Pirdavani, and A. P. C. Larocca, "Driver behavioral classification on curves based on the relationship between speed, trajectories, and eye movements: a driving simulator study," *Sustainability*, vol. 14, no. 10, p. 6241, 2022.

[47] J. A. Kim, J. Y. Sung, and S. H. Park, "Comparison of faster-RCNN, YOLO, and SSD for real-time vehicle type recognition," in *Proceedings of the 2020 IEEE International Conference on Consumer Electronics Asia*, Seoul, Korea, November 2020.

[48] X. Zhao, G. Wang, Z. He, and H. Jiang, "A survey of moving object detection methods: a practical perspective," *Neurocomputing*, vol. 503, pp. 28–48, 2022.

[49] M. Maity, S. Banerjee, and S. Sinha Chaudhuri, "Faster R-CNN and YOLO based vehicle detection: a survey," in *Proceedings of the 2021 5th International Conference on Computing Methodologies and Communication (ICCMC)*, pp. 1442–1447, Erode, India, April 2021.

[50] Y. Du, Z. Zhao, Y. Song et al., "StrongSORT: make DeepSORT great again," *IEEE Transactions on Multimedia*, vol. 25, pp. 8725–8737, 2023.

[51] K. T. Song and J. C. Tai, "Dynamic calibration of pan-tilt--zoom cameras for traffic monitoring," *IEEE Transactions on Systems, Man and Cybernetics, Part B (Cybernetics)*, vol. 36, no. 5, pp. 1091–1103, 2006.

[52] X. Zhang, Y. Feng, P. Angeloudis, and Y. Demiris, "Monocular visual traffic surveillance: a review," *IEEE Transactions on Intelligent Transportation Systems*, vol. 23, no. 9, pp. 14148–14165, 2022.

[53] N. K. Kanhere and S. T. Birchfield, "A taxonomy and analysis of camera calibration methods for traffic monitoring applications," *IEEE Transactions on Intelligent Transportation Systems*, vol. 11, no. 2, pp. 441–452, 2010.

[54] K. Wang, H. Huang, Y. Li, and F. Y. Wang, "Research on lane-marking line based camera calibration," in *Proceedings of the 2007 IEEE International Conference on Vehicular Electronics and Safety, ICVES*, Beijing, China, December 2007.

[55] X. Chen, Z. Li, Y. Yang, L. Qi, and R. Ke, "High-resolution vehicle trajectory extraction and denoising from aerial videos," *IEEE Transactions on Intelligent Transportation Systems*, vol. 22, no. 5, pp. 3190–3202, 2021.

[56] X. Shi, Y. D. Wong, M. Z. F. Li, and C. Chai, "Key risk indicators for accident assessment conditioned on pre-crash vehicle trajectory," *Accident Analysis & Prevention*, vol. 117, pp. 346–356, 2018.

[57] V. A. Bharat Kumar Anna, S. P. Venthuruthiyil, and M. Chunchu, "Vehicle trajectory data extraction from the horizontal curves of mountainous roads," *Transportation Letters*, vol. 15, no. 9, pp. 1055–1065, 2022.

[58] C. Zhang, Z. Tang, M. Zhang, B. Wang, and L. Hou, "Developing a more reliable aerial photography-based method for acquiring freeway traffic data," *Remote Sensing*, vol. 14, no. 9, p. 2202, 2022.

[59] Y. Yin, H. Wen, L. Sun, and W. Hou, "Study on the influence of road geometry on vehicle lateral instability," *Journal of Advanced Transportation*, vol. 2020, Article ID 7943739, 15 pages, 2020.

[60] Y. Chen, T. Shi, S. Yu, Q. Shi, J. He, and Y. Bian, "Setting the speed limit for highway horizontal curves: a revision of inferred design speed based on vehicle system dynamics," *Safety Science*, vol. 151, Article ID 105729, 2022.

[61] M. Alonso, D. A. Mántaras, and P. Luque, "Toward a methodology to assess safety of a vehicle," *Safety Science*, vol. 119, pp. 133–140, 2019.

[62] J. Morrall, R. T.-T. R. Record, and undefined, "Side friction demanded and margins of safety on horizontal curves," *Transportation Research Record*, vol. 2588, 1994.

[63] S. P. Venthuruthiyil and M. Chunchu, "Trajectory reconstruction using locally weighted regression: a new methodology to identify the optimum window size and polynomial order," *Transportmetrica: Transportation Science*, vol. 14, no. 10, pp. 881–900, 2018.

[64] L. Ebadi, H. Z. M. Shafri, S. B. Mansor, and R. Ashurov, "A review of applying second-generation wavelets for noise removal from remote sensing data," *Environmental Earth Sciences*, vol. 70, no. 6, pp. 2679–2690, 2013.

[65] J. Zhao, X. Yang, and C. Zhang, "Vehicle trajectory reconstruction for intersections: an integrated wavelet transform and Savitzky-Golay filter approach," *Transportmetrica: Transportation Science*, vol. 15, pp. 1–24, 2023.

[66] S. K. Srirangam, K. Anupam, A. Scarpas, C. Kasbergen, and M. Kane, "Safety aspects of wet asphalt pavement surfaces through field and numerical modeling investigations," *Transportation Research Record: Journal of the Transportation Research Board*, vol. 2446, no. 1, pp. 37–51, 2014.